Research on Engineering Structures & Materials
www.jresm.org
Research Group

ResearchArticle

Thermo-mechanical behavior of a symmetric single-walled carbon nanotube/polymer reinforced beam laminate

Sami Berrais [a], Sabiha Tekili [*,b], Abdelaziz Nehal [c], Youcef Khadri [d]

Advanced Technologies in Mechanical Production Research Laboratory(LRATPM), Faculty of Technology, Badji Mokhtar-Annaba university, P.O. Box 12, 23000, Annaba, Algeria

Article Info

Article History:

Received 24 July 2025

Accepted 03 Dec 2025

Keywords:

Carbon nanotubes;
Mori-Tanaka method;
Laminate beam;
Mechanical behavior;
Thermal behavior;
MATLAB

Abstract

The symmetrical laminates reinforced with carbon nanotubes (CNTs) offer exceptional performance,due to their high specific stiffness, low density, and excellent fracture toughness. Through theunderstanding of their thermo-mechanical behavior under various stresses and temperature is essential for their design. Moreover, if the distribution and orientation of CNTs are adjusted and their agglomeration is avoided, their integration into a polymer matrix allows the macroscopic application of their exceptional characteristics in different fields. This work provides a micromechanical modeling approach to predict the effective thermo-elasticbehavior ofnanocomposites. In order to determine these effective parameters,the Mori-Tanaka homogenization approach is used.with a volume fraction equal or less thanten percent which, modify significantly thermo-elastic properties of the composite and also, a simplified model where CNTs are modeled as hollow cylindrical shells.These effective properties are combined via MATLAB for ensuring a structural analysis based on the classical laminate theory and first-order shear deformation theory to examine the mechanical behavior and the classical laminate theory to evaluate the thermal behavior of symmetric laminated nanocomposite beams. The model focuses particularly on the thickness distribution of normal as in-plane and out-of-plane shear stresses that vary over thickness and stresses, deformations due to the temperature variation. The resultsshow the need to capture shear deformation effects and indicate the validity ofproposed model for analyzing stress continuity and identifying critical locations in nanocomposite laminates and so how each ply reacts to a temperature variation despite an overall geometry without curvature.

1. Introduction

Carbon nanotubes (CNTs) have been drawing continuing interest since their development in the early 1990s [1]. This is explained by their remarkable mechanical, electrical and thermal properties. Recent publications [2,3] have already established these features, making them interesting choices for composite reinforcement [4]. A little amount of CNTs can improve the overall thermo-elastic characteristics of the composite [5], which prompted the use of numerous frequent methodologies tostudythe thermo-elastic behavior of fiber-reinforced composites.In this side, Seidel and Lagoudas achieved it for carbon nanotube-reinforced composites (CNTRC) [6]. X. Li et al. obtained an excellent agreement between their simulation outcomes and experimental data when using self-consistent methods, as they combined it with Halpin-Tsai theory in their simulation of nanocomposites single-walled carbon nanotubes (SWCNTs)/Epoxy [7]. Z. He et al. obtained almost 20%ofreduction for the coefficient of thermal expansion and 40%.

*Corresponding author: sabiha.tikili@univ-annaba.dz
[a]orcid.org/0009-0009-9643-2222; [b]0009-0001-2261-375; [c]orcid.org/0009-0000-4579-8077
[d]orcid.org/0009-0000-6976-7195
DOI: http://dx.doi.org/10.17515/resm2025-1042ma0724rs

increasingthethermal conductivity by just adding 2% of weight of CNTs [8].Due to multiple variables that complicate the experimental field and the fact that the rule of mixtures (ROM) cannot be taking into account,some important parameters such as the agglomeration effect of CNTs [9] and since thatit's swift, operates oneasyanalytical approximations and doesn't ask moreof computational resources. Several writers [10, 11] choose the use of the Mori-Tanaka (MT) [12], which is regarded as one of the best analytical approaches for calculating the effective constants of the composite. At large scale, classical laminate theory (CLT) was employed to simulate multilayer structures, using the effective characteristics determined previously [13, 14]. Heshmati and Yas [15] also had combined the MT approach with a finite element method to analyze CNTs' agglomeration and dispersion effects on FG Euler–Bernoulli beams. Authors of [16] captured the CNTs agglomeration effects on Young's modulus, then utilized the non-linear von Kármán strain–displacement approximation to obtain the nonlinear strain of the continuous system via Euler-Bernoulli beam theory. At [17] Huang, X.-H et al. proposed an analytical model based on CLT to predict thermal expansion coefficients. By means of the Timoshenko beam model in [18], both the critical buckling resistance and post-buckling path of the multilayered beams generated from GPLR nanocomposites were examined. Dynamic modelling of the shafts was mainly carried out utilizing equivalent modulus beam theory (EMBT), where its formulation has been established based on the Timoshenko beam theory, as well as layer wisebeam theory (LBT) formulations [19]. Also, an FGM model was proposed with taking into account, volume fraction to study thermal bending with FSDT [20]. On the other hand, nonlinear dynamic and energetic assessments of multi-layer plates having an auxetic core were conducted by employing the nonlinear expansion of the kinematic equations of Reddy's higher-order shear deformation theory (HSDT) in [21]. The main objective for developing these advanced components is their application in structures, such as beams [22-24], plates [25, 26], shells [27] or in thermal environments [26, 27]. These constructions are subjected to different applied loads such as deflection [28], buckling [28-31], bending [29, 30] and stress [32-34]. Moreover, the calculation of stresses due to temperature variation which cause deformations on a microscopic scale, leads to residual stresses which can be significant for different phenomena [35]. In this work, a micromechanical modeling approach is adopted to calculate the effective elastic constants of SWCNTs-reinforced nanocomposite laminate. This approach uses MATLAB toward an accurate simple model where carbon nanotubes are modeled as hollow cylindrical shells [36]. In addition, the effective wall thickness of SWCNTs is limited to the value of $t = 0.142\ nm$, following the recommendation reported in [37]. The effective elastic properties are then used in first-order shear deformation theory (FSDT)to calculate the in-plane normal and shear stress,with out-of-plane shear stress distributions of the laminate, which is an essential step in evaluating the strength and stability of structures. By incorporating the effects of transverse shear deformation, the model enables more accurate stress predictions in medium-thickness laminates, where CLT may be insufficient. Also, the study of thermal constraints will not allowto harm the composite structures because of the difference between the thermal expansion coefficients of the matrix and the reinforcement. This multiscale framework thus provides a consistent and comprehensive representation of the thermo-mechanical behavior of CNTRC laminates, linking microscale interactions and macroscale structural response.

2.Elementary Equations

2.1. Mechanical Moments and Bending Stresses

The equations of a symmetric laminated beam are provided by [38] in order to determine the stress behavior of a laminated beam composed of carbon nanotube-based nanocomposite.

$$\begin{bmatrix} Mx \\ My \\ Mxy \end{bmatrix} = \begin{bmatrix} D_{11} & D_{12} & D_{16} \\ D_{12} & D_{22} & D_{26} \\ D_{16} & D_{26} & D_{66} \end{bmatrix} \begin{bmatrix} kx \\ ky \\ kxy \end{bmatrix} \quad (1)$$

kx, ky and kxy correspond to the curvatures, the flexural stiffnesses are $D_{ij=\,1,2,6}$and the flexural moments are Mx, My, and Mxy while Δ is the matrix $[D_{ij}]$ determinant and D_{11}^{*} is an element of the inverse matrix.

$$D_{11}^{*} = \frac{1}{\Delta}(D_{22}D_{66} - D_{26}^{2})$$
$$\Delta = D_{11}D_{22}D_{66} + 2\,D_{12}D_{16}D_{26} - D_{11}D_{26}^{2} - D_{22}D_{16}^{2} - D_{66}D_{12}^{2} \quad (2)$$

The bending occurs along the x axis here, where the bending and shear moments resolve to zero respectively

$$M_y = 0\ and\ \ M_{xy} = 0 \quad (3)$$

Then the deflection will only be a function of x

$$k_x = -\frac{d^2 w_0}{d_x^2} = D_{11}^{*} M_x \quad (4)$$

Since the $\frac{L}{b}$ratio is high enough, the equation (4) can be expressed as follows:

$$\frac{d\varphi_x}{dx} = \frac{d^2 w_0}{d_x^2} = -\frac{M}{E_x I} \quad (5)$$

Where M is the bending moment, I is the quadratic moment of the beam's cross-section with respect to the (x, y) plane, $E_x$is the flexural modulus of the beam and are written as:

$$E_x = \frac{12}{h^3 D_{11}^{*}}, \qquad I = I_{xy} = \frac{bh^3}{12}, \qquad M = bM_x \quad (6)$$

The stresses components within thek^{th} layer can be expressed as

$$\sigma_{xx}^{k} = z\, a_{xx}^{k} \frac{M}{I} \text{where} a_{xx}^{k} = \frac{h^3}{12}\sum_{j=1,2,6} Q_{1j}^{k} D_{1j}^{*} \quad (7)$$

$$\sigma_{yy}^{k} = z\, a_{yy}^{k} \frac{M}{I} \text{where} a_{yy}^{k} = \frac{h^3}{12}\sum_{j=1,2,6} Q_{2j}^{k} D_{1j}^{*} \quad (8)$$

$$\sigma_{xy}^{k} = z\, a_{xy}^{k} \frac{M}{I} \text{where} a_{xy}^{k} = \frac{h^3}{12}\sum_{j=1,2,6} Q_{6j}^{k} D_{1j}^{*} \quad (9)$$

While $L = 10mm, b = 1mm$ and $h = 1mm$ denote the length, width and the height of the laminated beam respectively and Q_{ij} represents the rigidity coefficients. The transverse shear stress is calculated by

$$\sigma_{xz}^{k} = -a_{xx}^{k}\tau_0 \left[4\left(\frac{z}{h}\right)^2 + d_k\right] \quad (10)$$

Such that, d_k is a constant which can be found as a first step by making σ_{xz}^{k} zero both the high and the belowsurfaces of the beam and guaranteeing that the lamina interfaces respect the continuity used. The maximum shear τ_0 is obtained at $z = 0$ and provided by

$$\tau_0 = \frac{3\left(\frac{dM}{dx}\right)}{2bh} \quad (11)$$

Assuming a load P who occurs on a simply supported beam at its midpoint, the maximum bending stress in the k^{th}layer of the symmetric laminated beam can be calculated by

$$\sigma_{xx}^{k} = -2\, a_{xx}^{k}\sigma_0 \frac{z}{h} \quad (12)$$

The maximum tensile stress $\sigma_0$which is found at $\left(z = -\frac{h}{2}\right)$ and the maximum shear stress which is given at $z = 0$ are respectively expressed to normalize the stress results

$$\sigma_0 = \frac{3PL}{2bh^2},\ \tau_0 = -\frac{3P}{4bh} \tag{13}$$

The elastic constant values are provided from [39] by

$$\begin{bmatrix}\sigma_{11}\\ \sigma_{22}\\ \sigma_{33}\\ \sigma_{23}\\ \sigma_{13}\\ \sigma_{12}\end{bmatrix} = \begin{bmatrix} n & l & l & 0 & 0 & 0\\ l & k+m & k-m & 0 & 0 & 0\\ l & k-m & k+m & 0 & 0 & 0\\ 0 & 0 & 0 & 2m & 0 & 0\\ 0 & 0 & 0 & 0 & 2p & 0\\ 0 & 0 & 0 & 0 & 0 & 2p \end{bmatrix} \begin{bmatrix}\varepsilon_{11}\\ \varepsilon_{22}\\ \varepsilon_{33}\\ \varepsilon_{23}\\ \varepsilon_{13}\\ \varepsilon_{12}\end{bmatrix} \tag{14}$$

According to [36], the Hill's elastic moduli are the constants k, l, m, n and $p$respectively represent, the transverse plane-strain bulk modulus, the transverse cross modulus, the transverse shear modulus, the axial tensile modulus and the axial shear modulus, which are calculated using the MT method as follows

$$k = \frac{E_m\{E_m c_m + 2k_r(1+v_m)[1+c_r(1-2v_m)]\}}{2(1+v_m)[E_m(1+c_r-2v_m)+2c_m k_r(1-v_m-2v_m^2)]} \tag{15}$$

$$l = \frac{E_m\{c_m v_m[E_m+2k_r(1+v_m)]+2c_r l_r(1-v_m^2)\}}{(1+v_m)[2c_m k_r(1-v_m-2v_m^2)+E_m(1+c_r-2v_m)]} \tag{16}$$

$$m = \frac{E_m[E_m c_m + 2m_r(1+v_m)(3+c_r-4v_m)]}{2(1+v_m)\{E_m[c_m+4c_r(1-v_m)]+2c_m m_r(3-v_m-4v_m^2)\}} \tag{17}$$

$$n = \frac{E_m^2 c_m(1+c_r-c_m v_m)+2c_m c_r(k_r n_r - l_r^2)(1+v_m)^2(1-2v_m)}{(1+v_m)\{2c_m k_r(1-v_m-2v_m^2)+E_m(1+c_r-2v_m)\}} + \frac{E_m[2c_m^2 k_r(1-v_m)+c_r n_r(1-2v_m+c_r)+4c_m c_r l_r v_m]}{2c_m k_r(1-v_m-2v_m^2)+E_m(1+c_r-2v_m)} \tag{18}$$

$$p = \frac{E_m[E_m c_m + 2(1+c_r)p_r(1+v_m)]}{2(1+v_m)[E_m(1+c_r)+2c_m p_r(1+v_m)]} \tag{19}$$

$$E_L = n - \frac{l^2}{k},\ E_T = \frac{4m(kn-l^2)}{kn-l^2+mn} \tag{20}$$

$$G_{LT} = 2p \text{ and } v_{LT} = \frac{l}{2k} \tag{21}$$

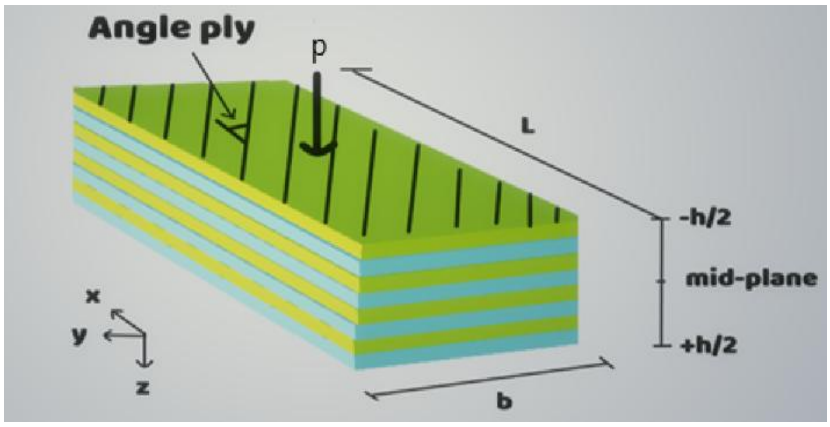

Fig. 1.Geometry of nanocomposite laminate beam in orthogonal axis

Due to the assumed small thickness of the plies, plane stress conditions are assumed in each ply, because of the assumed plane stress conditions, only four elasticity parameters E_L, E_T, G_{LT}, v_{LT}, which are related to the local axes of orthotropy, are necessary to define the elasticity matrix of the material [40]. Fig.1 displays more details of the laminate beam in an orthogonal axis.

2.2. Thermal Effects

The symmetric laminates are a good fit for the idea of determining its coefficients of thermal expansion since the coupling stiffness matrix $[B] = O$ and no bending happens under thermal stresses. Because thermal stresses in this kind of laminate produce zero resultant forces, the n-ply laminate is introduced by [41] as follows

$$[N^T] = \begin{bmatrix} N_x^T \\ N_y^T \\ N_{xy}^T \end{bmatrix} = \Delta T \sum_{k=1}^{n} \begin{bmatrix} \overline{Q_{11}} & \overline{Q_{12}} & \overline{Q_{16}} \\ \overline{Q_{12}} & \overline{Q_{22}} & \overline{Q_{26}} \\ \overline{Q_{16}} & \overline{Q_{26}} & \overline{Q_{66}} \end{bmatrix}_k \begin{bmatrix} \alpha_x \\ \alpha_y \\ \alpha_{xy} \end{bmatrix}_k (h_k - h_{k-1}) \tag{22}$$

While $[A_{ij}]$is the extensional matrix, $[N^T]$ is the resultants thermal force and moments (thermal moments $[M^T] = 0$ under uniform temperature variation at symmetric laminates) which is given by

$$\begin{bmatrix} N_x^T \\ N_y^T \\ N_{xy}^T \end{bmatrix} = \begin{bmatrix} A_{11} & A_{12} & A_{16} \\ A_{12} & A_{22} & A_{26} \\ A_{16} & A_{26} & A_{66} \end{bmatrix} \begin{bmatrix} \varepsilon_x^0 \\ \varepsilon_y^0 \\ \gamma_{xy}^0 \end{bmatrix} \tag{23}$$

Using the thermoelastic extremum principle, the laminate thermal expansion coefficients are developed by

$$\alpha_1 = \frac{1}{E_L}(\alpha_{cnt} E_{cnt} c_r + \alpha_m E_m c_m)\,, \alpha_2 = (1 + v_{cnt})\alpha_{cnt} c_r + (1 + v_m)\alpha_m c_m - \alpha_1 v_{LT} \tag{24}$$

The transformation matrix [T] must be added in order to determine the thermal expansion coefficients of each ply

$$\begin{bmatrix} \alpha_x \\ \alpha_y \\ \frac{\alpha_{xy}}{2} \end{bmatrix} = [T]^{-1} \begin{bmatrix} \alpha_1 \\ \alpha_2 \\ 0 \end{bmatrix} \tag{25}$$

The global strains in each laminate ply can be computed, the real strains in the laminate are represented by these global strains. However, mechanical strains are composed of the difference between the real strains and the free expansion strains. The k^{th} ply's mechanical strains are determined by

$$\begin{bmatrix} \varepsilon_x^M \\ \varepsilon_y^M \\ \gamma_{xy}^M \end{bmatrix} = \begin{bmatrix} \varepsilon_x \\ \varepsilon_y \\ \gamma_{xy} \end{bmatrix} - \begin{bmatrix} \varepsilon_x^T \\ \varepsilon_y^T \\ \gamma_{xy}^T \end{bmatrix} \tag{26}$$

The symbol M denote mechanical, T denote thermal while ΔT denote difference temperature, where the thermal and global strains are introduced by

$$\begin{bmatrix} \varepsilon_x^T \\ \varepsilon_y^T \\ \gamma_{xy}^T \end{bmatrix}_k = \Delta T \begin{bmatrix} \alpha_x \\ \alpha_y \\ \alpha_{xy} \end{bmatrix}_k \tag{27}$$

The thermal stresses in any ply are then given by

$$\begin{bmatrix} \sigma_x^T \\ \sigma_y^T \\ \tau_{xy}^T \end{bmatrix}_k = -\begin{bmatrix} \overline{Q_{11}} & \overline{Q_{12}} & \overline{Q_{16}} \\ \overline{Q_{12}} & \overline{Q_{22}} & \overline{Q_{26}} \\ \overline{Q_{16}} & \overline{Q_{26}} & \overline{Q_{66}} \end{bmatrix}_k \begin{bmatrix} \varepsilon_x^T \\ \varepsilon_y^T \\ \gamma_{xy}^T \end{bmatrix}_k = -\overline{Q_k} \,.\, \alpha_k^T \,.\, \Delta T \tag{28}$$

By applying the transformed reduced stiffness matrix to the mechanical strain vector, the mechanical stress components in the k^{th}ply of the laminate can be calculated as follows:

$$\begin{bmatrix}\sigma_x\\ \sigma_y\\ \tau_{xy}\end{bmatrix}_k = \begin{bmatrix}\overline{Q_{11}} & \overline{Q_{12}} & \overline{Q_{16}}\\ \overline{Q_{12}} & \overline{Q_{22}} & \overline{Q_{26}}\\ \overline{Q_{16}} & \overline{Q_{26}} & \overline{Q_{66}}\end{bmatrix}_k \begin{bmatrix}\varepsilon_x^M\\ \varepsilon_y^M\\ \gamma_{xy}^M\end{bmatrix}_k \tag{29}$$

3.Validation

As shown at fig.2, the present work has a relative deviation of 1.84% at the normalized normal stress and satisfy the boundary conditions at the normalized out-of-plane shear stress as [32]. A polystyrene matrix is the involved polymer matrix with a Young's modulus of $E_m = 1.9\ GPa$ and Poisson's ratio as $v^m = 0.3$, the diameters of the nanotubes are taken as $d = 0.2nm$, the wall thickness as $t = 0.142nm$, then, $k_r = 30\ GPa$, $l_r = 10\ GPa$, $m_r = p_r = 1\ GPa$, $n_r = 450\ GPa$ as Hill's elastic constants for a SWCNTs (10,10) with a volume fraction of $c_r = 10\%$.

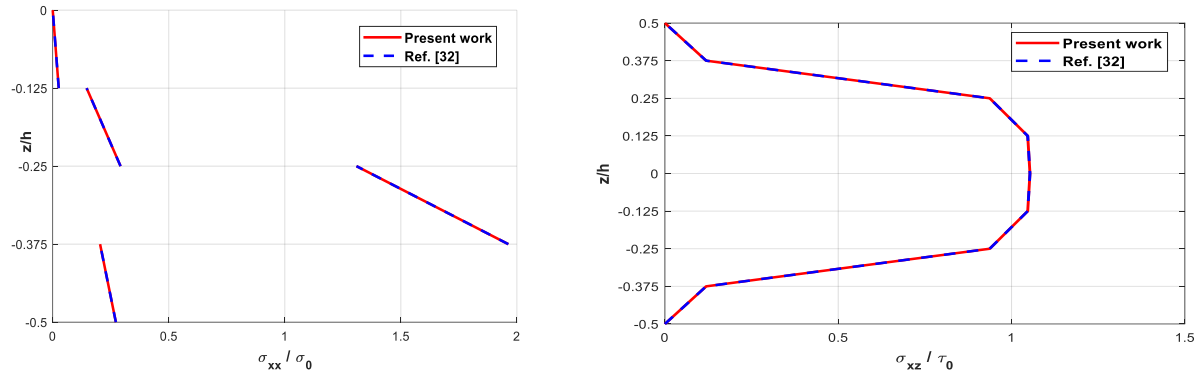

Fig. 2. A comparison of dimensionless normal and shear stresses alongside the normalized thickness of the laminate for a stacking sequence of $[45°/0°/-45°/90°]_s$ for present work and [32]

4. Results and Discussion

It is important to note that, in practice, CNTs concentrations dot not usually exceed 5~10%[42]. The reason is relatedto the fact that obtaining uniform filler dispersions at high concentrations is an intricate task due to the tendency of CNTs to agglomerate in bundles. For the CNTRC with various stacking sequences, the numerical calculationsusethe engineering constants that were taken from [43] to table 1. using the micromechanical equations that were mentioned above.

The variation of the normalized in-plane stresses (longitudinal, transverse and shear) by the maximum tensile stress with respect to $\frac{z}{h}$ is introduced in fig.3. A symmetric laminate with a stacking sequence of $[45°/0°/-45°/90°]_s$ is investigated. Where the composite contains the same polymer matrix and is reinforced with various materials, each with a volume fraction of $c_r = 10\%$. When all materials have the same geometry and are undergoing to the same external load P, a lower stress value doesn't necessarily mean that the ply is more resistant.

Table 1. Hill's elastic constants of constituent phases

	Graphene	Graphite	CNT
$k_r\ [GPa]$	850	620	30
$l_r\ [GPa]$	6.8	15	10
$n_r\ [GPa]$	102000	36.5	450
$m_r\ [GPa]$	369	440	1
$p_r\ [GPa]$	102000	4	1

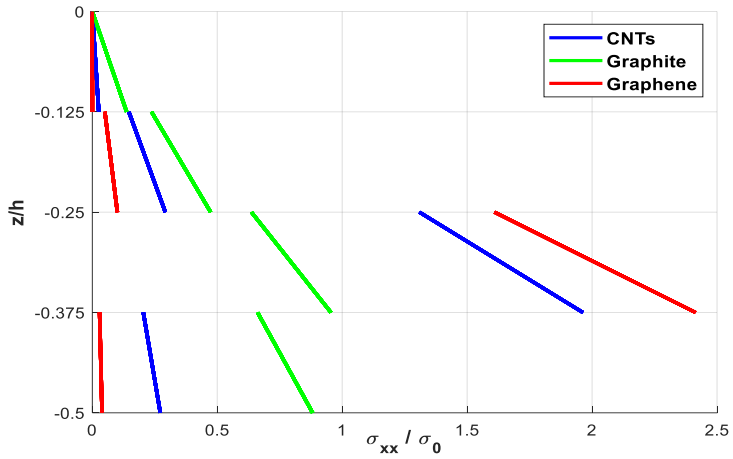

Fig. 3. Distribution of [45°/0°/-45°/90°]$_s$ for dimensionless normal stress across normalized thickness

In pure bending, CLT allows linearity in each layer of the laminate. in fig.3, the 0° layer, thanks to its high bending strengthe.g. approximately 8 times greater than that of the 45°-fold for CNTs, generates a lot of stress and can withstand a greater number of the bending force, making it the most stressed layer in tension/compression. The upper surface $z > 0$ is subjected to maximum compression, and the lower surface $z < 0$ to maximum tension. It is in this layer that the failure criteria will most often be verified first, as poor interlaminar behavior may be suspected. The behavior of the reinforcements, through the normalized stress $\frac{\sigma_{xx}}{\sigma_0}$, varies significantly depending on the orientation of the layers in the laminate. In ±45° orientations, the highest stress value in these folds is less than 1, which reflects a partial contribution of the reinforcements to longitudinal bending via coupling mechanisms.

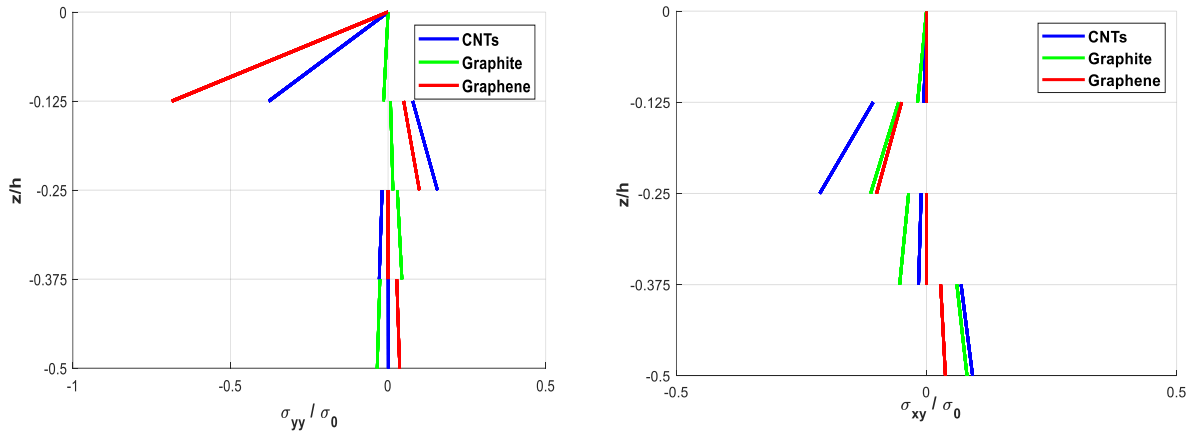

Fig. 4. Distribution of [45°/0°/-45°/90°]$_s$ for:a) dimensionless transverse stress across normalized thickness, b) dimensionless in-plane shear stress across normalized thickness

In contrast, in the 0° oriented layer, where the reinforcements are aligned with the bending direction, the stress peaks around 1, 2 and 2.5 for graphite, CNTs and graphene, respectively, indicating maximum reinforcement mobilization in longitudinal tension or compression. In the 90° layer, the stress drops back in value, the highest stress value of the three reinforcements does not even reach 0.25 in the bending direction. Since the main reinforcement is aligned in the x-plane for the 0° oriented layers and in the diagonal for the 45° layers. Then, there will be no bending in the y-plane. The main deformation is in ε_{xx}, so the σ_{yy}stresses will be closer tozero. As seen in fig. 4a. we can see also that these orientations do not mobilize the reinforcement in the y-axis. CNTs and graphene, being highly anisotropic, generate compressive transverse stresses in 90° folds, where the Poisson effect becomes dominant. The folds oriented at ±45° in fig. 4b. essentially generate the

normalized shear stress $\frac{\sigma_{xy}}{\sigma_0}$, in accordance with the symmetry of the stack and with opposite contributions in sign. The folds at 0° and 90° confirm the predominant role of the oblique layers in the transfer of σ_{xy} and induce stress values between 0.02 and -0.08.

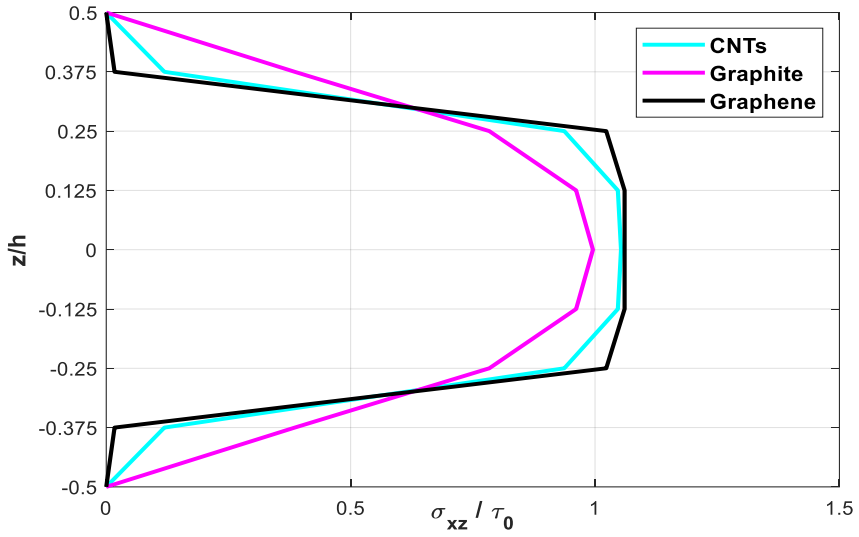

Fig. 5. Distribution of $[45°/0°/-45°/90°]_s$ for dimensionless out-of-plane shear stress across normalized thickness for various reinforcement

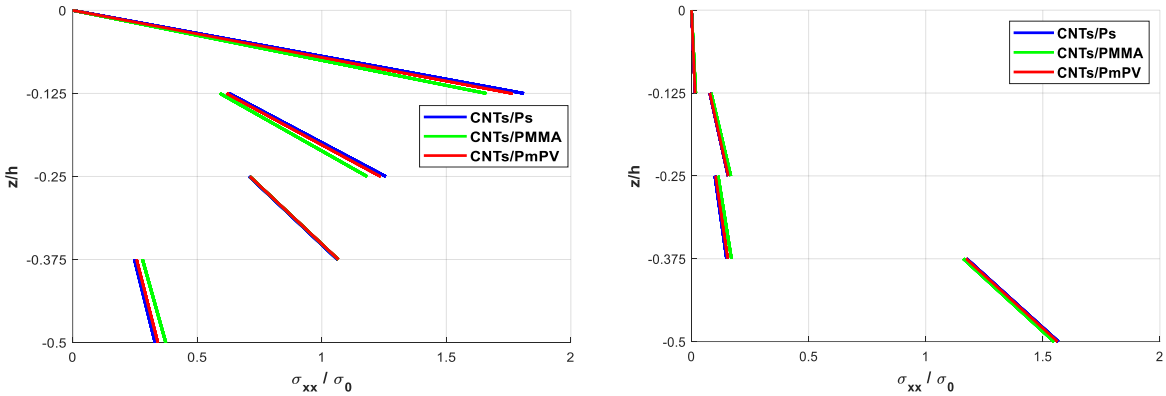

Fig. 6. Distribution of dimensionless normal stress across normalized thickness for a) a stacking sequence of $[90°/45°/-45°/0°]_s$, b) a stacking sequence of $[0°/45°/-45°/90°]_s$

The distribution of the out-of-plane shear stress normalized by the maximum shear stress with respect to $\frac{z}{h}$ is displayed in fig. 5 with the same properties as the laminate, which is displayed above in fig.3 and fig. 4. The coefficient $a_{xx}(k)$ acts as a local stiffness weight for each layer in Fig. 5, which shows a parabolic distribution of σ_{xz} in the thickness and vanishes at the edges.Graphene results show values ranging from 0 to 0.17 at the 45° bend and from 1.0229 to 1.0605 at the -45° bend, this behavior is expected since it is extremely stiff in in-plane tension, but weak in out-of-plane shear, especially in inclined orientations. CNTs behave better than graphene with out-of-plane transverse shear in ±45° bends and have the same behavior at 0° and 90° bends, they both have no contribution, while graphite is somewhat stable in all sequences. At the mid-plane, all reinforcements reach their maximum out-of-plane shear stresses.

At fig. 6 and fig. 7, a SWCNTs (10,10) volume fraction of $c_r = 10\%$ is mixed with different matrices on different stacking sequences: the polystyrene matrix, which is introduced above and two other matrices, which are polymeric, isotropic and possess identical Poisson's ratios $v^m = 0.34$, while the Young's modulus of the Poly(methyl methacrylate) (PMMA) matrix is$E_m = 2.5\ GPa$ and $E_m = 2.1\ GPa$ for the Poly(meta-phenylene vinylene-co-2,5-dioctoxy para-phenylene) (PmPV) matrix

[44]. The normal stresses σ_{xx}in each stacking sequence in fig. 6, are highly dependent on the ply orientation. Since the 0° layers are generally the ones which contribute the most to bending because the reinforcement there is aligned with the main load direction, these layers consequently experience higher normal stresses and significantly improve axial stiffness when they are located on the outside of the laminate, as in the $[0°/45°/-45°/90°]_s$ sequence. On the other hand, the centered position of the 0° layers in the $[90°/45°/-45°/0°]_s$ sequence limits their direct contribution to bending and favors a transfer of normal stresses to the inner layers.

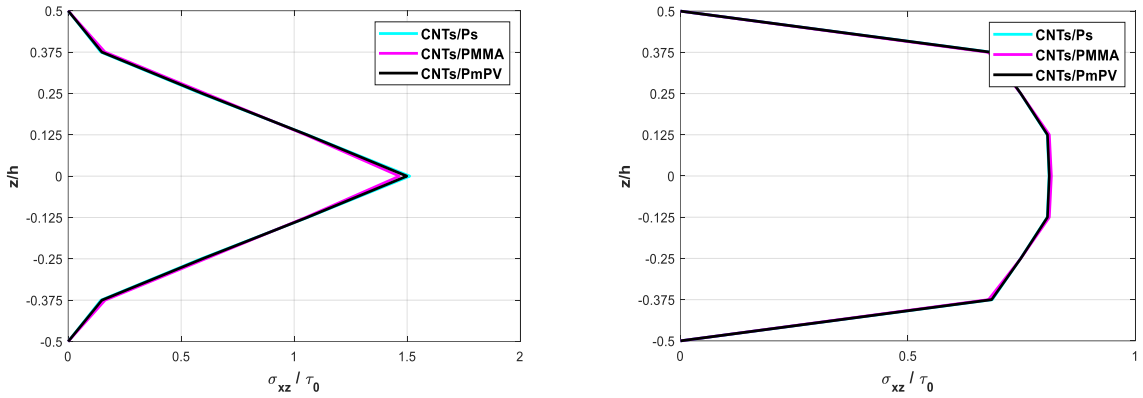

Fig. 7. Distribution of dimensionless out-of-plane shear stress across normalized thickness for : a) a stacking sequence of $[90°/45°/-45°/0°]_s$, b) a stacking sequence of $[0°/45°/-45°/90°]_s$

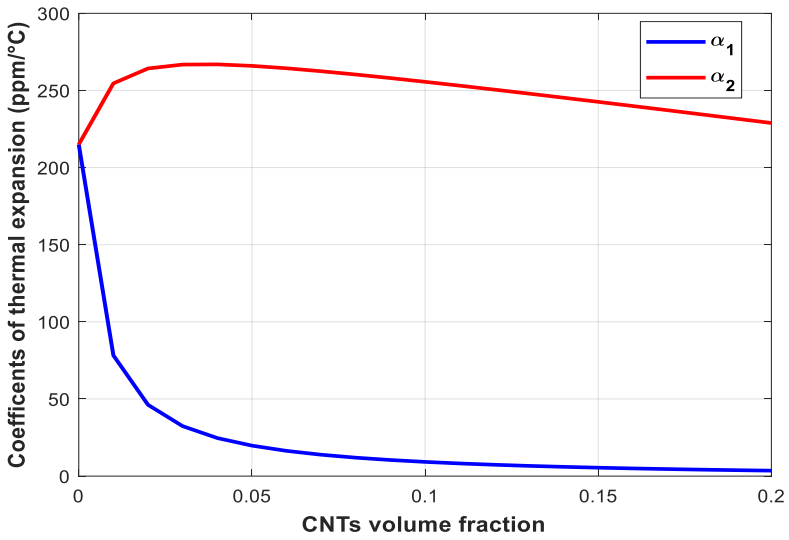

Fig. 8. Effect of CNTs volume fraction on longitudinal and transverse CTE

In Fig. 7, the matrix is highly stressed in 90° shear since the fibers do not support well the longitudinal loads. The results clearly indicate that the layers oriented at ± 45°, which, support the highest shear stresses, are less stressed in the stacking sequence of $[0°/45°/-45°/90°]_s$. Despite the difference in stiffness of the three matrices, PS being the softest, PMMA being the stiffest and PmPV being intermediate, there is almost no big difference in response to stresses. The reinforcement dominates the mechanical behavior and the matrix has little influence at out-of-plane shear stress.

The variation in length per unit of variation in temperature is known as the coefficient of thermal expansion (CTE). For a laminate with a stacking sequence of $[0°/\overline{90°}]_s$, three coefficients of thermal expansion are defined: $\alpha_x$in the x-direction, $\alpha_y$in the y-direction, α_{xy}in the x-y-plane direction. Assuming that $\alpha_{cnt} = -0.9\ x\ 10^{-6}(K^{-1})$ at room temperature is the CTE for the reinforcing phase, SWCNTs (10, 10) [45]. While $\alpha_m = 215\frac{ppm}{°C}$ at 29.9°C is the CTE of the PMMA matrix [46], its glass transition temperature T_g, which separates two regimes of the polymer behavior, justifies the

relation; $T < T_g$, the CTE of the matrix can be taken as $\alpha_m = 215\,\frac{ppm}{°C}$. Because α_m remainsconstant from 10°C to 80°C, the variation of temperature is taken as $\Delta T = 70°C$. The longitudinal, transverse CTE, Young's modulus and Poisson's ratio of the laminate are respectively calculated as $\alpha_1 = 9.22\ X\ 10^{-6}K^{-1}$, $\alpha_2 = 2.556\ X\ 10^{-4}K^{-1}$, $E_L = 46.634\ GPa$ and $v_{LT} = 0.3883$, where Young's modulus and Poisson's ratio of CNTs are taken from [47] as $E_{cnt} = 600\ GPa$ and $v_{cnt} = 0.19$ while CNTs volume fraction is taken as $V_{cnt} = 10\%$. The transformed coefficients of thermal expansion are

$$\begin{bmatrix}\alpha_x\\ \alpha_y\\ \alpha_{xy}\end{bmatrix}_{0°} = \begin{bmatrix}9.22\ X\ 10^{-6}\\ 2.556\ X\ 10^{-4}\\ 0\end{bmatrix}K^{-1}, \begin{bmatrix}\alpha_x\\ \alpha_y\\ \alpha_{xy}\end{bmatrix}_{90°} = \begin{bmatrix}2.556\ X\ 10^{-4}\\ 9.22\ X\ 10^{-6}\\ 0\end{bmatrix}K^{-1} \tag{30}$$

The variation of both longitudinal and transverse CTE of the laminate as a function of CNTs volume fraction is illustrated in fig. 8. The longitudinal direction in the lamina, which is aligned with the orientation of the CNTs, shows a significant reduction in $\alpha_1$despite the matrix being highly thermally expansive. This behavior results from the negative CTE of the CNTs and their high axial stiffness, which allows them to have a significant impact in the effective response through a stiffness-weighted averaging. In contrast, α_2 is only slightly reduced, since the matrix governs the transverse properties due to the low volume fraction and limited transverse stiffness of the CNTs.

Table 2. Distribution of strains in a $[0°/\overline{90°}]_s$laminate with respect to z under a temperature change of 70°C

Ply no.	ε_x	ε_x^T	ε_x^M	ε_y	ε_y^T	ε_y^M	$\gamma_{xy}, \gamma_{xy}^T, \gamma_{xy}^M$
1 (0°)		6.454 X 10^{-4}	0.0013		0.0179	-0.0142	0
2 (90°)	0.001946	0.0179	-0.016	0.003691	6.454 X 10^{-4}	0.003	0
3 (0°)		6.454 X 10^{-4}	0.0013		0.0179	-0.0142	0

Considering the thermal expansion coefficients and mechanical stiffness of each layer, the strains of each ply for a symmetric laminate with a stacking sequence of $[0°/\overline{90°}]_s$are evaluated in tab. 2. The composite composedof SWCNTs (10,10) as a reinforcement and PMMA as a matrix. Since there are no mechanical loads, there is only a constant variation of temperature in all the laminate. There will be no thermal bending moments $[M]^T = 0$ and no curvatures $[k] = 0$. Then, through the thickness, the mid-plane stain remains constant and the same strain occurs in every lamina. Since, the CTEs are different in the fiber and transverse directions. Thermal stresses vary depending on the ply orientation, which allows for the calculation of mechanical deformations.

Table 3. Distribution of stresses in a $[0°/\overline{90°}]_s$laminate with respect to z under a temperature change of 70°C

Ply no.	$\sigma_x[MPa]$	$\sigma_x^T[MPa]$	$\sigma_y\ [MPa]$	$\sigma_y^T[MPa]$	$\sigma_{xy}, \sigma_{xy}^T$
1 (0°)	45.8058	−49.728	−38.1546	−50.545	0
2 (90°)	−41.33	−50.545	123.85	−49.728	0
3 (0°)	45.8058	−49.728	−38.1546	−50.545	0

These thermal strains, denoted ε^T, are computed from the temperature change and the effective CTE of each layer and generate internal stresses even in the absence of external mechanical loads. The analysis of tab. 3. shows that even with a uniform-imposed deformationε^0, the mechanical stresses vary according to ε^T, which depends on the bend angle. The 0° and 90° bends are the most constrained bends, because the greater the difference between ε^0 and ε^T, the higher the mechanical stresses will be. The negative sign for the stresses indicates that there is compressive stress.Fig.9

shows the linear distribution of normal thermal stress due to a temperature variation of 70°; it is constant in the 0° bends and changes by approximately 1.64% in the 90° bend.

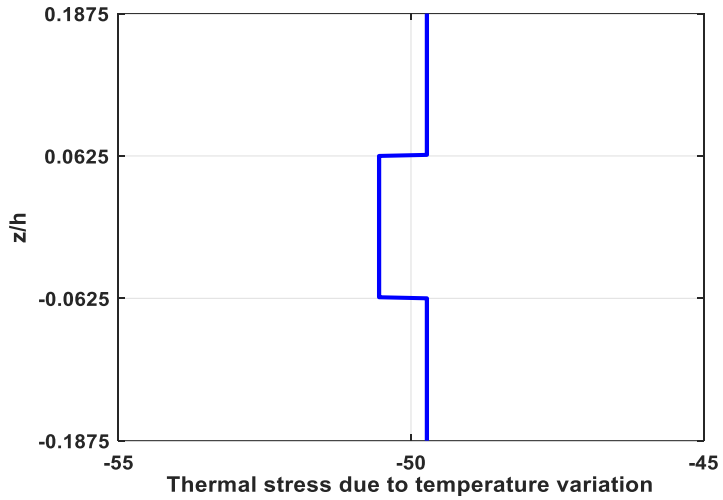

Fig. 9. Thermal stress σ_x^T distribution across laminate thicknessfor a stacking sequence of $[0°/\overline{90°}]_s$

5. Conclusions

To evaluate the elastic response of CNT-reinforced nanocomposite beams, a multiscale analytical model was developed using effective properties derived from the Mori-Tanaka homogenization method. With the help of MATLAB, the structural behavior of the beams was analyzed at the macroscopic scale, although its reinforcement occurs at the nanoscale, reflecting its applicability to real-scale engineering systems in many fields such as defense, aeronautics, automotive and civil engineering.Using a parabolic distribution across the normalized thickness, the out-of-plane transversestresswascalculated by FSDT theory, which takes into account the transverse shear effects neglected by CLT. The obtained results illustrate the impact of the reinforcement volume fraction and stacking sequences on the mechanicalperformance of the reinforced laminate beam. A moderate quantity of CNTs can improve the mechanical, thermal response of the structure. On the other hand, the arrangement of the layers strongly affects the stress distribution, while placing the 0° layers on the outside allows for better axial load support and consistent bending behavior. Also, the matrix plays a more important role than the fibers in sequences where the reinforcements are not aligned with the primary load direction. The results sheds light on the anisotropic response of reinforcements, where they contribute strongly to the normal stress in 0° bends, moderately at ±45° and almost without any contribution at 90°. The analysis of thermal strains and global stresses due to temperature variation in a symmetric laminate involves understanding how each ply reacts to difference of temperature despite an overall geometry without curvature. Moreover, increasing the volume fraction of CNTs in a polymer matrix will lead to a marked reduction in the longitudinal thermal expansion coefficient α_1, making the composite more thermally stable in the principal direction. While results show the poor thermal behavior at the transverse direction, there is not an important change in the transversal thermal expansion coefficient α_2. Finally, The MATLAB implementation created, will serve as a flexible framework for upcoming investigations on non-symmetric laminates, higher-order shear deformation theories, and various composite geometries.

Acknowledgement

This research has been conducted within a PRFU project 2020-2025. The authors would like to express their gratitude for all the people who provided us with advice and support throughout this study.

References

[1]Iijima S. Helical microtubles of graphitic carbon. Nature. 1991;354:56-58. https://doi.org/10.1038/354056a0

[2] Ince Yardimci A, et al. SEM images of carbon nanotubes (CNTs): effect of voltage and spot size on image resolutions. Research & Design. 2024;1(1):43-51. https://doi.org/10.17515/rede2024-004en1116rs

[3] Sahai RS, et al. Study on performance of multiwall carbon nanotubes and functionalized multiwall carbon nanotubes/ poly aryl ether ketone polymer composite gears. Res Eng Struct Mater. 2025;11(1):273-285.http://dx.doi.org/10.17515/resm2024.217na0324rs

[4] Pak SY, et al. Micro-Macroscopic coupled modeling for the prediction of synergistic improvement on the thermal conductivity of boron nitride and multi-walled carbon nanotube reinforced composites. Compos Part A. 2021;148:106474. https://doi.org/10.1016/j.compositesa.2021.106474

[5] Mesfin KK, Ananda BA, Tilak R. Three-phase modelling and characterization of elastic behavior of MWCNT reinforced GFRP composites: A combined numerical and experimental study. Mater Today Proc. 2020;26:944-949. https://doi.org/10.1016/j.matpr.2020.01.152

[6] Seidel G, Lagoudas D. Micromechanical analysis of the effective elastic properties of carbon nanotube reinforced composites. Mech Mater. 2006;38(8-10):884-907. https://doi.org/10.1016/j.mechmat.2005.06.029

[7] Li X, et al. Reinforcing mechanisms of single-walled carbon nanotube-reinforced polymer composites. J Nanosci Nanotechnol. 2007;7(7):2309-2317. https://doi.org/10.1166/jnn.2007.410

[8] He Z, et al. Insight into the mechanical properties and thermal expansion behavior of epoxy nanocomposites reinforced with multi-walled carbon nanotube solvent-free nanofluids. Polym Compos. 2024;45(5):4401-4411. https://doi.org/10.1002/pc.28069

[9] Heshmati M, Yas MH. Free vibration analysis of functionally graded CNT-reinforced nanocomposite beam using Eshelby-Mori-Tanaka approach. J Mech Sci Technol. 2013;27(11):3403-3408. https://doi.org/10.1007/s12206-013-0862-8

[10] Skocek J, Zeman J, Sejnoha M. Effective properties of textile composite: application of the Mori-Tanaka method. Model Simul Mater Sci Eng. 2008;16(8):085002-15. https://doi.org/10.1088/0965-0393/16/8/085002

[11] Fedotov A. A numerical-analytical model of elasto-plastic deformation of matrix composites. Acta Mech. 2024;235:3633-3642. https://doi.org/10.1007/s00707-024-03918-x

[12] Mori T, Tanaka K. Average stress in matrix and average elastic energy of materials with misfitting inclusions. Acta Metall. 1973;21:571-574. https://doi.org/10.1016/0001-6160(73)90064-3

[13] Ghorbanpour Arani A, Maghamikia S, Mohammadimehr M, Arefmanesh A. Buckling analysis of laminated composite rectangular plates reinforced by SWCNTs using analytical and finite element methods. J Mech Sci Technol. 2011;25(3):809-820. https://doi.org/10.1007/s12206-011-0127-3

[14] Tahouneh V, Naei MH. Using Eshelby-Mori-Tanaka sheme for 3D free vibration analysis of sandwich curved panels with functionally graded nanocomposite face sheets and finite length. Polym Compos. 2016. https://doi.org/10.1002/pc.23929

[15] Heshmati M, Yas MH. Free vibration analysis of functionally graded CNT-reinforced nanocomposite beam using Eshelby-Mori-Tanaka approach. J Mech Sci Technol. 2013;27:3403-3408. https://doi.org/10.1007/s12206-013-0862-8

[16] Dabbagh A, Ebrahimi F. Postbuckling analysis of meta-nanocomposite beams by considering the CNT's agglomeration. Eur Phys J Plus. 2021;136:1168. https://doi.org/10.1140/epjp/s13360-021-02160-x

[17] Huang XH, et al. A comparative analysis of thermo mechanical behavior of CNT reinforced composite plates: Capturing the effects of thermal shrinkage. Case Stud Therm Eng. 2022;38. https://doi.org/10.1016/j.csite.2022.102347

[18] Yang J, Wu H, Kitipornchai S. Buckling and postbuckling of functionally graded multilayer graphene platelet-reinforced composite beams. Compos Struct. 2017;161:111-118. https://doi.org/10.1016/j.compstruct.2016.11.048

[19] Udatha P, Sekhar AS, Velmurugan R. Eigen value analysis of composite hollow shafts using modified EMBT formulation considering the shear deformation along the thickness direction. DefTechnol. 2023;28:1-12. https://doi.org/10.1016/j.dt.2022.12.020

[20] Li J, et al. Thermomechanical bending of functionally graded carbon nanotubes reinforced composite plate by mechless method. Polym Compos. 2024;45(14):13063-13075. https://doi.org/10.1002/pc.28686

[21] Zhu X, Zhang J, Zhang W, Chen J. Vibration frequencies and energies of an auxetic honeycomb sandwich plate. Mech Adv Mater Struct. 2019;26(23):1951-1957. https://doi.org/10.1080/15376494.2018.1455933

[22] Vo-Duy T, Ho-Huu V, Nguyen-Thoi V. Free vibration analysis of laminated FG-CNT reinforced composite beams using finite element method. Front Struct Civ Eng. 2019;13:324-336. https://doi.org/10.1007/s11709-018-0466-6
[23] Shafiei H, Setoodeh AR. An analytical study on the nonlinear forced vibration of functionally graded carbon nanotube-reinforced composite beams on nonlinear viscoelastic foundation. Arch Mech. 2020;72:81-107.
[24] Civalek Ö, Akbas S, Akgöz B, Dastjerdi S. Forced vibration analysis of composite beams reinforced by carbon nanotubes. Nanomaterials. 2021;11:571. https://doi.org/10.3390/nano11030571
[25] Wu CP, Chang SK. Stability of carbon nanotube-reinforced composite plates with surface-bonded piezoelectric layers and under bi-axial compression. Compos Struct. 2014;111:587-601. https://doi.org/10.1016/j.compstruct.2014.01.040
[26] Ebrahimi F, Nouraei M, Dabbagh A, Rabczuk T. Thermal buckling analysis of embedded grapheneoxide powder-reinforced nanocomposite plates. Adv Nano Res. 2019;7(5):293-310.
[27] Shen H. Torsional postbuckling of nanotube-reinforced composite cylindrical shells in thermal environments. Compos Struct. 2014;116:477-488. https://doi.org/10.1016/j.compstruct.2014.05.039
[28] Akbas SD. Post-buckling analysis of a fiber reinforced composite beam with crack. Eng Fract Mech. 2019;212:70-80. https://doi.org/10.1016/j.engfracmech.2019.03.007
[29] Chitour M, et al. A Novel high order theory for static bending of functionally graded (FG) beams subjected to various mechanical loads. Res Eng Struct Mater. 2024;10(4):1523-1539. https://doi.org/10.17515/resm2024.141me0104rs
[30] Polit O, Anant C, Anirudh B, Ganapathi M. Functionally graded graphene reinforced porous nanocomposite curved beams: Bending and elastic stability using a higher order model with thickness stretch effect. Compos B Eng. 2019;166:310-327. https://doi.org/10.1016/j.compositesb.2018.11.074
[31] Amani MA, Ebrahimi F, Dabbagh A, Rastgoo A, Nasiri MM. A machine learning-based model for the estimation of the temperature-dependent moduli of graphene oxide reinforced nanocomposites and its application in a thermally affected buckling analysis. Eng Comput. 2021;37(3):2245-2255. https://doi.org/10.1007/s00366-020-00945-9
[32] Wuite J, Adali S. Deflection and stress behaviour of nanocomposite reinforced beams using a multiscale analysis. Compos Struct. 2005;71:388-396. https://doi.org/10.1016/j.compstruct.2005.09.011
[33] Akmal J, et al. Development and validation of an accurate analytical solution for hoop stress distribution in cylindrical functionally graded materials. Res Eng Struct Mater. 2025;11(5):2521-2535. https://doi.org/10.17515/resm2025-777an0324rs
[34] Patton A, Faroughi S, Reali A. Efficient equilibrium-based stress recovery for isogeometric laminated Euler-bernoulli curved beams. Compos Struct. 2024;118374. https://doi.org/10.1016/j.compstruct.2024.118374
[35] Shokrieh MM. Residual stresses in composite materials. Woodhead Publishing Series in Composites Science and Engineering; 2014. No. 48. https://doi.org/10.1533/9780857098597.1.173
[36] Khaldi A, Tekili S, Khadri Y. Vibration of nanocomposite beams reinforced by SWCNTs under the action of harmonic load. Res Eng Struct Mater. 2025. http://dx.doi.org/10.17515/resm2025-1013ma0706rs
[37] Vodenitcharova T, Zhang LC. Effective wall thickness of a single-walled carbon nanotube. Phys Rev B. 2003;68:165401. https://doi.org/10.1103/PhysRevB.68.165401
[38] Berthelot JM. Composite materials, mechanical behaviour and structural analysis. New York: Springer-Verlag; 1999. https://doi.org/10.1007/978-1-4612-0527-2
[39] Popov VN, Doren VE, Balkanski M. Elastic properties of crystals of single-walled carbon nanotubes. Solid State Commun. 2000;114:359-399. https://doi.org/10.1016/S0038-1098(00)00070-3
[40] Altenbach H, Öchsner A. Encyclopedia of Continuum Mechanics. Springer Nature; 2019. https://doi.org/10.1007/978-3-662-53605-6
[41] Estrada H, Lee L. Mechanics of composite materials. In: The international handbook of FRP composites in civil engineering. 2013. p. 51-78.
[42] Coleman JN, Khan U, Blau WJ, Gun'ko YK. Small but strong: A review of the mechanical properties of carbon nanotube-polymer composites. Carbon. 2006;44:1624-1652. https://doi.org/10.1016/j.carbon.2006.02.038
[43] G-Macias E, R-Tembleque L, Saez A. Bending and free vibration analysis of functionally graded graphene vs. carbon nanotube reinforced composite plates. Compos Struct. 2017.
[44] Garcia-Macias E, Guzmán CF, Saavedra Flores EI, Castro-Triguero R. Multiscale modeling of the elastic moduli of CNT-reinforced polymers and fitting of efficiency parameters for the use of the extended rule-of-mixtures. Compos Part B Eng. 2019:114-131. https://doi.org/10.1016/j.compositesb.2018.09.057
[45] Shirasu K, Yamamoto G, Hashida T. Application of aligned carbon nanotube-reinforced polymer composite to electrothermal actuator. Carbon nanotubes- current progress of their polymer composites; 2016. https://doi.org/10.5772/62509

[46] Zhi CY, Bando Y, Wang WL, Tang CC, Kuwahara H, Golberg D. Mechanical and thermal properties of polymethyl Methacrylate-BN nanotube composites. J Nanomater. 2008. https://doi.org/10.1155/2008/642036

[47] Kamarian S, Shakeri M, Yas M, et al. Free vibration of functionally graded nanocomposite sandwich beams resting on Pasternak foundation by considering the agglomeration effect of CNTs. J Sandw Struct Mater. 2015;17:632-665. https://doi.org/10.1177/1099636215590280